

# Virtual touch tissue imaging quantification shear wave elastography for determining benign versus malignant cervical lymph nodes: a comparison with conventional ultrasound

Alican Kılıç   
Hale Çolakoğlu Er 

## PURPOSE

We aimed to prospectively examine virtual touch tissue imaging quantification (VTIQ) shear wave elastography (SWE) and conventional (B-mode and Doppler) ultrasonography (US), individually and combined, for their ability to differentiate benign and malignant cervical lymph nodes (CLNs).

## METHODS

One hundred enlarged lymph nodes (LNs) from 72 patients, confirmed by histopathologic diagnoses, were included in the present study. B-mode US, Doppler US, and SWE were performed before histopathologic sampling of the LNs. The LN shear wave velocity (SWV, m/s) was assessed by VTIQ.

## RESULTS

Using a 3.03 m/s cutoff value, the sensitivity, specificity, positive predictive value (PPV), negative predictive value (NPV), and accuracy of  $SWV_{max}$  for differentiating benign and malignant CLNs were 93%, 59%, 68%, 91%, and 75%, respectively. B-mode and Doppler had a sensitivity, specificity, PPV, NPV, and accuracy of 79.2%, 71.2%, 71.6%, 78.7%, and 75%, respectively. B-mode, Doppler, and VTIQ SWE combined had 87.5%, 75%, 76.3%, 86.6%, and 81% for the same parameters, respectively.

## CONCLUSION

VTIQ SWE is a promising noninvasive diagnostic imaging technique for differentiating benign and malignant CLNs. VTIQ SWV can improve the diagnostic performance of conventional US for differentiating benign and malignant CLNs.

The correct identification of distended lymph nodes (LNs) is difficult but essential and aids in patient prognosis and treatment options (1, 2). Conventional ultrasonography (US) has been used extensively for preoperative imaging and diagnosing malignant cervical lymph nodes (CLNs). Since the clinical application of ultrasound elasticity, it was used for distinguishing malignant and benign lesions at many sites. Several studies have shown that this technique positively correlates with histopathologic data (3–5).

Presently, quantitative techniques for elasticity include elastic tissue diffusion and acoustic radiation force impulse (ARFI) imaging (6). Virtual touch tissue imaging quantification (VTIQ) was developed and based on ARFI. VTIQ can be used to record multipoint shear wave velocity (SWV) with a wider range and a smaller region of interest (ROI) sampling frame (7–9). Studies evaluating CLNs with VTIQ shear wave elastography (SWE) and B-mode US are present in the literature (10–12). However, to our knowledge, Doppler US, VTIQ, and detailed B-mode features have not been evaluated altogether prospectively for distinguishing enlarged CLNs. The goal of the present study was to prospectively examine VTIQ SWE and B-mode and Doppler US, individually and combined, for their ability to differentiate benign and malignant CLNs.

## Methods

### Study population

Subjects were incorporated into this prospective study based on their referral to our radiology department between February 2018 and April 2018 for US examination and SWE

From the Department of Radiology (H.Ç.E. ✉  
halecolakoglu83@yahoo.com), Gaziantep University  
School of Medicine, Gaziantep, Turkey.

Received 12 September 2018; revision requested 23  
October 2018; last revision received 11 December  
2018; accepted 13 December 2018.

Published online 6 February 2019.

DOI 10.5152/dir.2019.18406

You may cite this article as: Kılıç A, Çolakoğlu Er H. Virtual touch tissue imaging quantification shear wave elastography for determining benign vs malignant cervical lymph nodes: a comparison with conventional ultrasound. *Diagn Interv Radiol* 2019; 25:114–121.

before US-guided fine-needle or excisional biopsy. Exclusion criteria were LNs with nondiagnostic cytopathologic results. One hundred enlarged LNs from 72 consecutive patients (36 males and 36 females; mean age, 45.9±21.3 years; range, 2–91 years) were recruited for the study. Our reference standard was the cytopathologic results. Written informed consent was obtained from the patients before the start of the study. Our institution's ethics committee approved the study in accordance with the Declaration of Helsinki (decision no.: 2018/26).

### US examination

The subjects were positioned supinely, while the neck was rested on a pillow. The examination started with B-mode and Doppler US, followed by VTIQ SWE. US and SWE were both performed using an Acuson S2000 US System (Siemens Medical). Conventional US imaging was done by using a 5.5–18 MHz 18L6 HD probe. LN level, short-axis diameter, axial ratio (short to long axis), presence or absence of the echogenic hilus, calcification, or cystic change, as well as LN vascularity pattern, were assessed in conventional examination. LN locations were classified as anatomic levels 1, 2, 3, 4, 5, and 6. According to this classification, level 1 LNs were submental and submandibular; level 2 LNs were upper internal jugular chain nodes; level 3 LNs were middle internal jugular chain nodes; level 4 LNs were lower internal jugular chain nodes; level 5 LNs were spinal accessory chain nodes and transverse cervical chain nodes; and level 6 LNs were anterior cervical nodes (13).

With color Doppler, the vascular pattern of the LN was evaluated as avascular, hilar, peripheral, and mixed (peripheral and hilar). The avascular and hilar patterns were defined as LNs with normal vascularity pattern, and the peripheral or mixed pattern as LNs with abnormal vascularity pattern.

### Shear wave elastography

An image was generated using a 4–9 MHz 9L4 probe combined with VTIQ. On the VTIQ, the probe was situated on the skin vertically and administered using minimal pressure. This was done to generate LN contact while the patient held his/her breath without swallowing. In the image, high-quality sections presented as green, low-quality sections presented as orange, and marginal-quality sections presented as yellow (14). Following this, the VTIQ velocity mode was switched. In the new mode, hard sections presented as red, medium-hard sections presented as yellow or green, and soft region sections presented as blue. A ROI was placed at the cortex of the LN (avoiding calcifications and cystic regions) on the color-coded map to acquire SWV. In the highest quality regions, SWV was measured using a fixed dimension ROI of 1.5×1.5 mm in the stiffest area within the LN. The highest velocity was defined as  $SWV_{max}$ . The arithmetic mean of three SWV values was defined as the  $SWV_{mean}$ .

### Pathologic diagnoses

After US elastography, all LNs were confirmed histopathologically by fine-needle and/or excisional biopsy.

### Statistical analysis

All analyses were performed using SPSS v.22 (SPSS Inc.). Measurements were expressed as mean±SD. Fisher's exact test and  $\chi^2$  test were used to determine the significant gray scale features and vascular patterns. Shapiro–Wilk test was used to evaluate data normality. Mann–Whitney U test was used to compare the non-normal distributed data between malignant and benign LNs. The ability of the SWV values, short-axis diameter, and axial ratio to dis-

tinguish malignant versus benign LNs was assessed using a receiver operating characteristic (ROC) curve. Cutoff values were acquired by Youden's index from the ROC curve. The sensitivity, specificity, positive predictive value (PPV), negative predictive value (NPV), and accuracy value were calculated for each predictor. A *P* value <0.05 was accepted as significant.

## Results

Of 100 LNs, 52 were benign (24 reactive lymphoid hyperplasia, 16 tuberculous lymphadenitis, 9 chronic inflammation, and 3 foreign body reaction), and 48 were malignant (33 metastases and 15 lymphomas). Metastases were classified as squamous cell carcinoma (n=10), papillary thyroid carcinoma (n=10), adenocarcinoma (n=9), malignant mesenchymal tumor (n=2), neuroendocrine tumor (n=1), and malignant histiocytic neoplasm (n=1).

Of the LNs, 18 were diagnosed only by fine-needle biopsy, 39 by fine-needle and excisional biopsy, and 43 by excisional biopsy.

B-mode US findings demonstrate most (42.3%) of the benign LNs at level 1, and some (31.3%) malignant LNs at level 2. The distribution of the LNs based on the American Joint Committee on Cancer LN classification is shown in Table 1.

The benign LNs' diameter of the short-axis varied from 4 to 29 mm (mean, 10.19±5.13 mm). The malignant LNs' short-axis diameter was from 7 to 30 mm (mean, 14.83±5.30 mm).

Using the ROC curve obtained from our data, the cutoff value for short-axis diameter was 10.5 mm for predicting malignant LNs at all LN levels. The sensitivity, specificity, PPV, NPV, and accuracy were 75%, 71%, 70%, 75%, and 73%, respectively (*P* < 0.001). The area under the curve (AUC) was 0.76 (95% confidence interval [CI], 0.67–0.86).

### Main points

- The SWV value of malignant lymph nodes was significantly higher than that of benign lymph nodes.
- A single cutoff value of 3.03 m/s was determined for distinguishing benign and malignant cervical lymph nodes using ROC curves.
- The combined use of VTIQ and conventional US had higher overall values than the conventional US.

**Table 1.** Lymph node levels based on the American Joint Committee on Cancer classification

Level	Benign (n=52), n (%)	Malignant (n=48), n (%)
1	22 (42.3)	11 (22.9)
2	13 (25)	15 (31.3)
3	2 (3.8)	4 (8.3)
4	4 (7.7)	7 (14.6)
5	11 (21.2)	9 (18.8)
6	0 (0)	2 (4.2)

The axial ratio of the benign LNs was 0.25 to 1.0 (mean, 0.57±0.17). The malignant LN axial ratio was 0.34 to 0.92 (mean, 0.67±0.14).

A cutoff value of 0.56 had the best sensitivity of 83.33%, which was based on the ROC curve. AUC was 0.70 (95% CI, 0.60–0.80). The specificity, PPV, NPV, and accuracy were 53.85%, 62%, 77%, and 68%, respectively ( $P < 0.001$ ).

Echogenic hilus was observed in 30 of 52 benign LNs (57.7%) and 8 of 48 malignant LNs (16.7%). The sensitivity, specificity, PPV, NPV, and accuracy of the echogenic hilus

were determined to be 83.3%, 57.6%, 64.5%, 78.9%, and 70%, respectively ( $P < 0.001$ ).

Calcification of benign and malignant LNs was not found to be significant ( $P = 0.83$ ). The sensitivity, specificity, PPV, NPV, and accuracy of calcification for predicting malignancy were 22.9%, 78.8%, 50%, 52.5%, and 52%, respectively.

The sensitivity, specificity, PPV, NPV, and accuracy of cystic changes to distinguish benign and malignant LNs were determined as 58.3%, 80.7%, 73.6%, 67.7%, and 70%, respectively ( $P < 0.001$ ). All B-mode US findings are detailed in Table 2.

Doppler US showed avascular pattern in 13 LNs, of which 9 (69.2%) were benign and 4 (30.8%) were malignant. Hilar pattern was seen in 26 LNs, of which 24 (92.3%) were benign and 2 (4.2%) were malignant. With color Doppler, the vascularity pattern of the LN for predicting malignancy had 87.5% sensitivity. The specificity, PPV, NPV, and accuracy were 63.4%, 68.8%, 84.6%, and 75%, respectively ( $P < 0.001$ ).

VTIQ SWE determined the SWV<sub>mean</sub> value of malignant LNs (4.18±1.10 m/s; range, 1.99–6.16 m/s) to be significantly higher than that of benign LNs (2.96±1.15 m/s;

**Table 2.** The distribution of findings according to benign/malignant lymph nodes and statistical data for conventional US characteristics and VTIQ SWV for predicting malignant lymph nodes

Variable	Benign LN (n=52), n (%)	Malignant LN (n=48), n (%)	Sensitivity (%)	Specificity (%)	PPV (%)	NPV (%)	Accuracy (%)	P
Short-axis diameter								
<10.5 mm	37 (71.1)	12 (25)	75	71	70	75	73	0.001
≥10.5 mm	15 (28.8)	36 (75)						
Axial ratio								
<0.56	24 (46.1)	8 (16.6)	83.3	53.8	62	77	68	0.001
≥0.56	28 (53.84)	40 (83.3)						
Echogenic hilus								
Present	30 (57.7)	8 (16.7)	83.3	57.6	64.5	78.9	70	0.001
Absent	22 (42.3)	40 (83.3)						
Calcification								
No	41 (78.8)	37 (77.1)	22.9	78.8	50	52.5	52	0.83
Yes	11 (21.2)	11 (22.9)						
Cystic changes								
No	42 (80.8)	20 (41.7)	58.3	80.7	73.6	67.7	70	0.001
Yes	10 (19.2)	28 (58.3)						
Vascularity pattern								
Normal	33 (63.4)	6 (12.5)	87.5	63.4	68.8	84.6	75	0.001
Abnormal	19 (36.5)	42 (87.5)						
SWV <sub>mean</sub>								
<3.03 m/s	33 (63.7)	4 (8.4)	91.6	63.4	69	89	77	0.001
≥3.03 m/s	19 (36.3)	44 (91.6)						
SWV <sub>max</sub>								
<3.03 m/s	31 (56.7)	3 (6.25)	93	59	68	91	75	0.001
≥3.03 m/s	21 (40.3)	45 (93.75)						

US, ultrasonography; VTIQ, virtual touch tissue imaging quantification; SWV, shear wave velocity; LN, lymph node; PPV, positive predictive value; NPV, negative predictive value.

**Table 3.** Conventional US, VTIQ SWE, and combined evaluation parameters

Modality	Sensitivity (%)	Specificity (%)	PPV (%)	NPV (%)	Accuracy (%)	P
Conventional US	79.2	71.2	71.6	78.7	75	0.001
VTIQ SWE	91.6	63.4	69	89	77	0.001
Conventional US+VTIQ SWE	87.5	75	76.3	86.6	81	0.001

US, ultrasonography; VTIQ, virtual touch tissue imaging quantification; SWE, shear wave elastography; PPV, positive predictive value; NPV, negative predictive value.

71.2%, 71.6%, 78.7%, and 75%, respectively. The same parameters mentioned above for the combined evaluation of VTIQ SWE and conventional US for distinguishing benign and malignant LNs were calculated as 87.5%, 75%, 76.3%, 86.6%, and 81%, respectively. These results are shown in Table 3. Figs. 2–4 show the examples of conventional US and VTIQ SWE findings.

## Discussion

The VTIQ SWV value of malignant LNs was significantly higher than that of benign LNs. A single cutoff value of 3.03 m/s was determined for distinguishing benign and malignant CLNs using ROC curves. AUCs for  $SWV_{mean}$  and  $SWV_{max}$  were 0.792 (95% CI, 0.702–0.883) and 0.788 (95% CI 0.697–0.879), respectively. Using a 3.03 m/s cutoff value, the sensitivity, specificity, PPV, NPV, and accuracy of VTIQ SWV for distinguishing benign and malignant CLNs were 91.6%, 63.4%, 69%, 89%, and 77%, respectively. Using the same cutoff value, the sensitivity, specificity, PPV, NPV, and accuracy of  $SWV_{max}$  for distinguishing benign and malignant CLNs were 93%, 59%, 68%, 91%, and 75%, respectively. The combined use of VTIQ and conventional US had higher sensitivity, specificity, PPV, NPV, and accuracy values (87.5%, 75%, 76.3%, 86.6%, and 81%, respectively) than the conventional US (79.2%, 71.2%, 71.6%, 78.7%, and 75%, respectively).

In previous studies, several cutoff values (5 mm, 8 mm, and 10 mm) were reported for the short-axis diameter in the differentiation of benign and malignant LNs (15–17). In our study, the best cutoff value determined by ROC analysis for all LNs was calculated as 10.5 mm (AUC, 0.764; 95% CI, 0.671–0.858). For the 10.5 mm cutoff value, the sensitivity, specificity, PPV, NPV, and accuracy were 75%, 71%, 70%, 75%, and 73%, respectively.

LN morphology is a useful criterion for distinguishing benign and malignant LNs. LN shape is determined by the axis ratio (short-axis/long axis). Different cutoff values have been reported for different regions of the neck with 0.5 being the most commonly used cutoff value for benign and malignant LN discrimination (18, 19). In our study, the best cutoff value for the axial ratio determined by ROC analysis was 0.56 (AUC, 0.70; 95% CI, 0.60–0.80), yielding 68% diagnostic accuracy. In the study by Ying et al. (19), the accuracy reported for 0.5 axial ratio of different neck levels in distinguish-

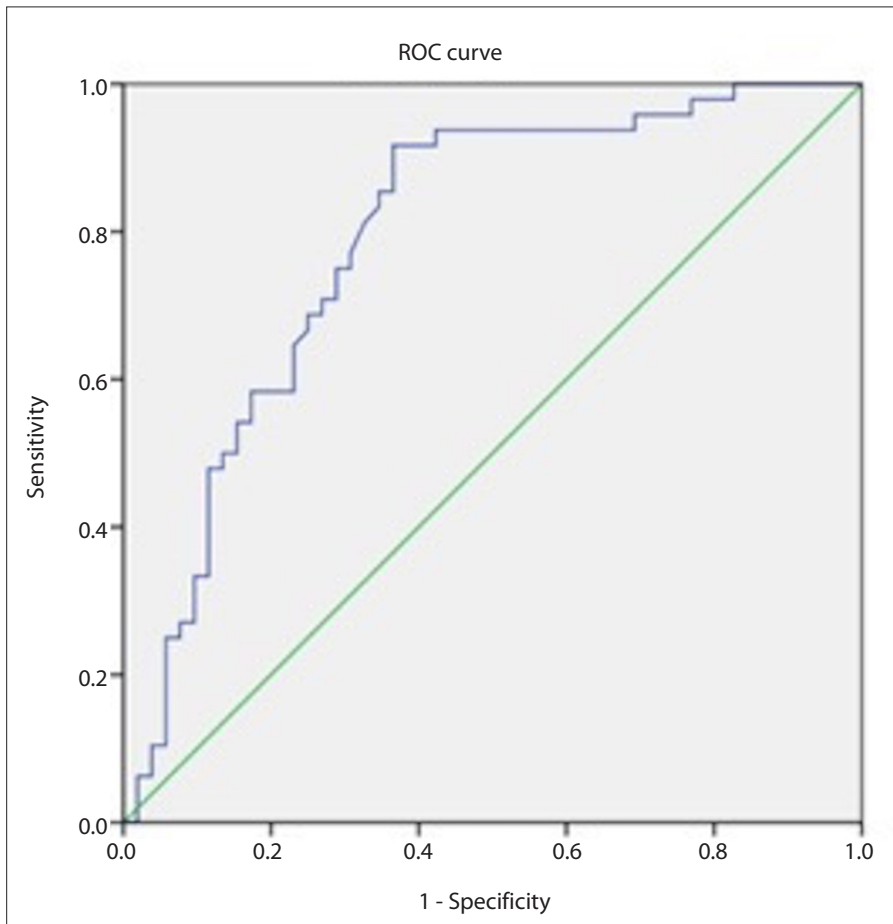


**Figure 1.** The ROC curve of  $SWV_{mean}$ . AUC was 0.792 (95% CI, 0.702–0.883).

range, 1.25–6.21 m/s). The  $SWV_{max}$  value of malignant LNs ( $4.51 \pm 1.16$  m/s; range, 2.1–6.41 m/s) was higher than that of benign LNs ( $3.21 \pm 1.23$  m/s; range, 1.33–6.25 m/s) ( $P < 0.001$ ). Using ROC curves, 3.03 m/s was determined as a single cutoff for differentiating benign and malignant CLNs. AUCs for  $SWV_{mean}$  and  $SWV_{max}$  were 0.792 (95% CI, 0.702–0.883) and 0.788 (95% CI, 0.697–0.879), respectively. Fig. 1 shows the ROC curve of  $SWV_{max}$ . Using a 3.03 m/s cutoff value, the sensitivity, specificity, PPV, NPV, and accuracy of VTIQ  $SWV_{mean}$  for dis-

tinguishing benign and malignant CLNs were 91.6%, 63.4%, 69%, 89%, and 77%, respectively. Using a 3.03 m/s cutoff value, the sensitivity, specificity, PPV, NPV, and accuracy of  $SWV_{max}$  for distinguishing benign and malignant CLNs were 93%, 59%, 68%, 91%, and 75%, respectively. The details are shown in Table 2.

The sensitivity, specificity, PPV, NPV, and accuracy of conventional US (B-mode and Doppler) for distinguishing benign and malignant LNs were calculated as 79.2%,

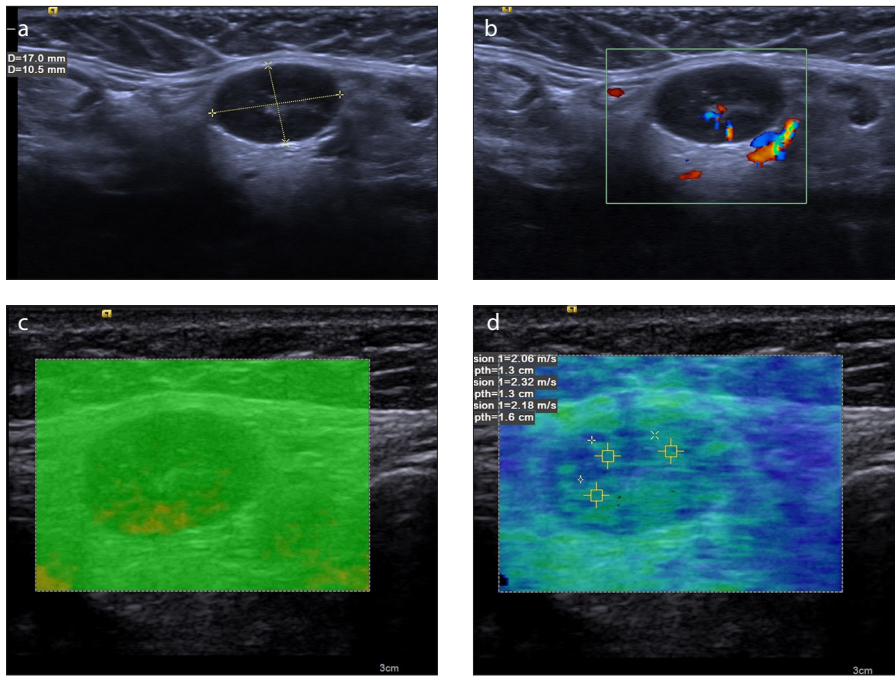


**Figure 2. a–d.** A 56-year-old woman with reactive LN. B-mode US image (a) reveals a 17×10.5 mm ovoid nodule with fatty hilus and 0.58 axial ratio at level 1. Normal hilar vascularization is seen on color Doppler (b). The VTIQ quality map (c) is green, indicating decent VTIQ estimates. VTIQ velocity mode image (d) shows the SWVs (m/s) of three different points.

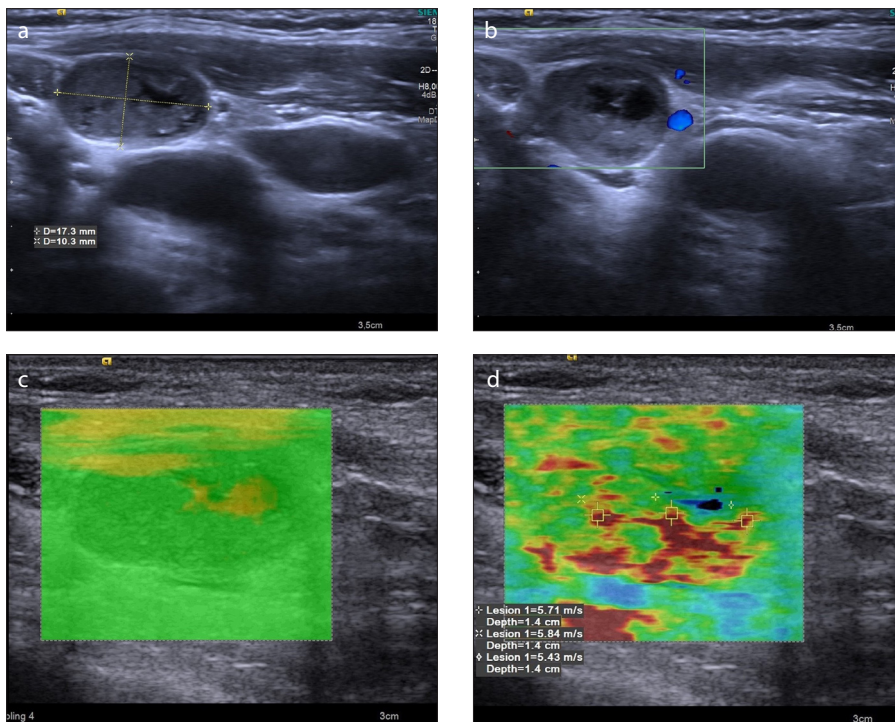


**Figure 3. a–d.** A 69-year-old man with metastatic LN from squamous cell carcinoma. B-mode US image (a) reveals a 17.3×10.3 mm lymph node with cystic changes, loss of echogenic hilus, and 0.59 axial ratio at level 2. Avascular pattern is seen in color Doppler (b). The VTIQ quality map (c) is green, indicating decent VTIQ estimates. VTIQ velocity mode image (d) shows the SWVs (m/s) of three different points.

ing malignant and benign LNs ranged from 66% to 90%, and sensitivity ranged from 22% to 93%. Alam et al. (20) reported 56%

accuracy for 0.6 axial ratio, and Lyshchik et al. (21) reported 79% accuracy for 0.5 axial ratio.

The occurrence of a central echogenic hilus in the LNs is generally thought to be a benign feature (22). In the studies performed by Ahuja et al. (23–28), metastatic, lymphomatous, and tuberculosis LNs did not have a hilus, whereas normal LNs typically had one. In our study, the accuracy of the echogenic hilus was calculated as 70%, and having an echogenic hilus was a statistically significant feature for distinguishing benign and malignant LNs ( $P < 0.001$ ). In the present study, the echogenic hilus was observed in 16.7% ( $n=8$ ) of malignant LNs and 57.7% ( $n=30$ ) of benign LNs. Of the LNs, 68% (15/22) without an echogenic hilus were histopathologically reported as granulomatous lymphadenitis. The precision of the echogenic hilus for distinguishing benign and malignant LNs was reported as 62% in the report by Lyshchik et al. (21) and 86% in the report by Alam et al. (20). However, the echogenic hilus has been observed in both benign and malignant LNs. The occurrence of the echogenic hilus cannot be the only benchmark for evaluating CLNs.

Nodal calcification commonly occurs in the metastatic thyroid nodes from papillary and medullary carcinoma (29). In our study, the accuracy of calcification for predicting malignancy was 52%. We found that the occurrence of calcification in the LN for distinguishing benign and malignant LNs was not statistically significant ( $P = 0.83$ ). In the study performed by Lyshchik et al. (21), the accuracy of calcification for predicting malignancy was reported as 59%, and this value is similar to the value in our study.

Cystic changes are usually seen in squamous cell carcinoma metastases (30), papillary thyroid carcinoma metastases (26), and tuberculous adenitis (24). Regardless of the nodal size, the LNs with intranodal necrosis should be considered pathologic. In the study by Azizi et al. (11), cystic content predicted malignant LN with a sensitivity of 22.22% and specificity of 98.1%. In our study, the sensitivity and specificity of cystic changes to distinguish benign and malignant LNs were determined to be 58.3% and 80.7%, respectively ( $P < 0.001$ ). Histopathologic identification of benign LNs with cystic change ( $n=10$ ) was reported as granulomatous lymphadenitis in our study.

Normal and reactive LNs appear to exhibit hilar vascularity or avascularity (31). Nevertheless, malignant nodes appear to be of peripheral or mixed vascularity (32). In our study, the avascular and hilar patterns were

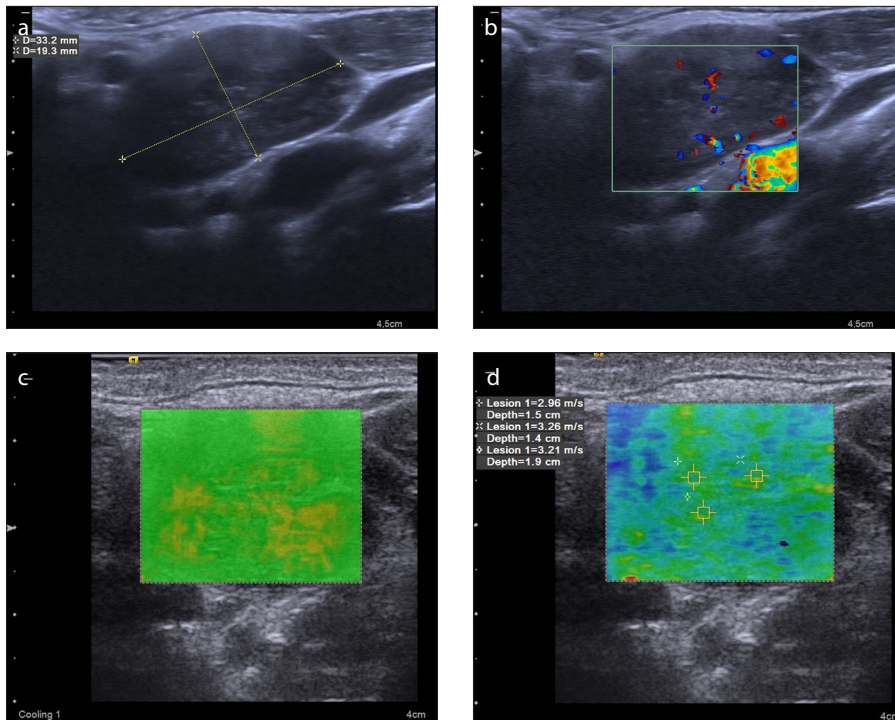


**Figure 4. a–d.** A 49-year-old man with Hodgkin lymphoma. B-mode US image (a) reveals a 33.2×19.3 mm lymph node with heterogeneous internal structure, loss of echogenic hilus, and 0.58 axial ratio at level 3. Abnormal mixed type vascularity pattern is seen on color Doppler (b). The VTIQ quality map (c) is green, indicating decent VTIQ estimates. VTIQ velocity image (d) shows the SWVs (m/s) of three different points. Histopathologic diagnosis was made after excisional lymph node biopsy because the lymph node could not be diagnosed by fine-needle aspiration biopsy.

defined as LNs with normal vascularity pattern, and the peripheral or mixed pattern as LNs with abnormal vascularity pattern. Of 19 benign LNs with abnormal vascularity, tuberculous lymphadenitis was diagnosed in 73.6% (n=14), chronic inflammation was diagnosed in 15.7% (n=3), and foreign body reaction was diagnosed in 10.7% (n=2). Doppler ultrasonography evaluation of nodal vascular pattern has been reported to have increased sensitivity (83%–89%) and specificity (87%–100%) for differentiating metastatic and reactive nodes (33–35). In the study performed by Lyshchik et al. (21), the sensitivity and specificity of vascularity to distinguish benign and malignant LNs were 47% and 99%, respectively. In our study, the vascularity pattern of the LN for predicting malignancy had a sensitivity of 87.5% and a specificity of 63.4%. The lower specificity value determined in our study was thought to be due to granulomatous LNs showing variable vascular pattern characteristics.

In our study, the  $SWV_{mean}$  value of malignant LNs ( $4.18 \pm 1.10$  m/s; range, 1.99–6.16 m/s) was significantly higher than that of benign LNs ( $2.96 \pm 1.15$  m/s; range, 1.25–6.21

m/s). The  $SWV_{max}$  value of malignant LNs ( $4.51 \pm 1.16$  m/s; range, 2.1–6.41 m/s) was significantly higher than that of benign LNs ( $3.21 \pm 1.23$  m/s; range, 1.33–6.25 m/s) ( $P < 0.001$ ). In our study, similar statistical methods were used with other studies evaluating VTIQ, and similarly, the ROC curve was generated to determine the optimal SWV cutoff value for differentiating benign and malignant CLNs (9–12). In a single cutoff analysis for predicting malignancy, 3.03 m/s was determined to be the threshold to distinguish benign and malignant CLNs using ROC curves. AUCs for  $SWV_{mean}$  and  $SWV_{max}$  were 0.792 (95% CI, 0.702–0.883) and 0.788 (95% CI, 0.697–0.879), respectively. Using a 3.03 m/s cutoff value, the sensitivity, specificity, PPV, NPV, and accuracy of  $SWV_{mean}$  for distinguishing benign and malignant CLNs were 91.6%, 63.4%, 69%, 89%, and 77%, respectively. Using the same cutoff value, the sensitivity, specificity, PPV, NPV, and accuracy of  $SWV_{max}$  for distinguishing benign and malignant CLNs were 93%, 59%, 68%, 91%, and 75%, respectively. Cheng et al. (9) showed that a cutoff value of 3.34 m/s results in benign and malignant discrimination (AUC, 0.855; 95% CI, 0.770–0.917),

with 78.9% sensitivity and 74.7% specificity. In the study by Zhang et al. (36), AUC was 0.838 with a 3.14 m/s cutoff value; sensitivity and specificity for benign and malignant discrimination were found as 77.1% and 85.7%, respectively. Azizi et al. (11) reported 92.5% sensitivity, 75.4% specificity, 48.5% PPV, and 97.6% NPV with a cutoff value of 2.93 m/s (AUC, 0.88; 95% CI, 0.82–0.93). The 3.03 m/s cutoff value determined in our study is near these cutoff values. In the meta-analysis by Zhang et al. (37) about the overall performance of ARFI for classifying LNs, they found that ARFI has a high accuracy for the identification of benign and malignant LNs with a pooled sensitivity of 87% and specificity of 88% and a corresponding AUC of 0.93. In the meta-analysis study conducted by Suh et al. (38), in which SWE techniques (ARFI and supersonic shear imaging) were evaluated, SWE showed a sensitivity and specificity of 81% and 86%, respectively (AUC, 0.85; 95% CI, 0.81–0.88). Compared with these values, the specificity and AUC for SWV was lower in our study, but the sensitivity was higher (especially for  $SWV_{max}$ ).

In the present study, the false positive results based on  $SWV_{max}$  and  $SWV_{mean}$  values were 21 (40.3%) and 19 (36.5%), respectively. Thirteen (61.9%) false positive LNs according to  $SWV_{max}$  and 13 (68.4%) false positive LNs according to  $SWV_{mean}$  were reported as granulomatous LNs. The three false positive LNs ( $SWV_{max}$  14.2% and  $SWV_{mean}$  15.7%) were foreign body reaction with dense fibrosis; two ( $SWV_{max}$  9.5% and  $SWV_{mean}$  10.5%) were chronic inflammation. Three (14.2%)  $SWV_{max}$  and one (5.2%)  $SWV_{mean}$  false positive LN measurements were reactive hyperplasia. In the study by Cheng et al. (9), 50% of tuberculous lymphadenitis and approximately 10% of reactive hyperplasia cases contributed to false positive outcomes based on VTIQ SWE. Similar to Cheng et al. (9), we also suggest that various structures, such as calcification and fibrosis, may yield false positivity. The low specificity values determined in our study were thought to be due to a large number of granulomatous LNs mimicking malignant tissue features in our study. There were 3 false negative results for  $SWV_{max}$  and 4 false negative results for  $SWV_{mean}$ , which were histopathologically diagnosed as Hodgkin lymphoma mixed cellularity type. Desmoplastic reaction that is observed in nodular sclerosing lymphoma and mixed cellular type lymphoma occurs predominantly in the late stages of the disease (39).

The LNs that yielded false negative results had not developed fibrosis tissue associated with desmoplastic reaction as confirmed by pathologic findings.

VTIQ does not depend on the ability of the operator to maintain optimal pressure. For evaluating the CLNs, VTIQ achieves intermediate to excellent interobserver and intraobserver reproducibility (9, 40). In addition, since VTIQ provides quantitative information about tissue stiffness, it has a clear superiority than strain elastography, which provides semiquantitative information.

In our study, the combined use of VTIQ and conventional US had higher overall values than the conventional US. In parallel with most of the studies in the literature, our study also showed that SWE is a highly sensitive technique for correct characterization of the enlarged CLNs especially when combined with conventional US. We think that the routine use of SWE may provide information about the LN characterization, reduce fine-needle biopsies, and the number of surgical excision cases. We also think that SWE will provide additional information to assess suspicious LNs and in cases where histopathologic evaluation is needed in the prognosis and staging of head and neck malignancies.

The present study has some limitations. First, we had a relatively small sample size. Second, a small variety of LNs were studied. The usefulness of VTIQ in LNs with diverse histology must be evaluated in further studies. Third, confirmation by histology was a part of our inclusion criteria. Similar to other studies, this may lead to a selection bias.

In conclusion, the SWV value of malignant LNs was significantly higher than that of benign LNs. In a single cutoff analysis, the best SWV for distinguishing benign and malignant CLNs was 3.03 m/s with a sensitivity of 93%. VTIQ could be used to evaluate the enlarged LNs and provide additional information to conventional US. Additionally, patients could avoid the possible complications of biopsy and surgery. We think that further studies with larger sample size and greater variety of LNs are required to validate our findings.

#### Conflict of interest disclosure

The authors declared no conflicts of interest.

#### References

1. Ying L, Hou Y, Zheng HM, Lin X, Xie ZL, Hu YP. Real-time elastography for the differentiation of benign and malignant superficial lymph nodes: a meta-analysis. *Eur J Radiol* 2012; 81:2576–2584. [\[CrossRef\]](#)
2. Serifoglu I, Oz, Il, Damar M, Tokgoz O, Yazgan O, Erdem Z. Diffusion-weighted imaging in the head and neck region: usefulness of apparent diffusion coefficient values for characterization of lesions. *Diagn Interv Radiol* 2015; 21:208–214. [\[CrossRef\]](#)
3. Klotz T, Boussion V, Kwiatkowski F, et al. Shear wave elastography contribution in ultrasound diagnosis management of breast lesions. *Diagn Interv Imaging* 2014; 95:813–824. [\[CrossRef\]](#)
4. Shi Y, Wang XH, Zhang HH, et al. Quantitative analysis of real-time tissue elastography for evaluation of liver fibrosis. *Int J Clin Exp Med* 2014; 7:1014–1021.
5. Han R, Li F, Wang Y, Ying Z, Zhang Y. Virtual touch tissue quantification (VTQ) in the diagnosis of thyroid nodules with coexistent chronic autoimmune Hashimoto's thyroiditis: a preliminary study. *Eur J Radiol* 2015; 84:327–331. [\[CrossRef\]](#)
6. Fu Y, Shi YF, Yan K, Wang YJ, Yang W, Feng GS. Clinical value of real time elastography in patients with unexplained cervical lymphadenopathy: quantitative evaluation. *Asian Pac J Cancer Prev* 2014; 15:5487–5492. [\[CrossRef\]](#)
7. Ianculescu V, Ciolovan LM, Dunant A, et al. Added value of Virtual Touch IQ shear wave elastography in the ultrasound assessment of breast lesions. *Eur J Radiol* 2014; 83:773–777. [\[CrossRef\]](#)
8. Liu H, Zhao LX, Xu G, et al. Diagnostic value of virtual touch tissue imaging quantification for benign and malignant breast lesions with different sizes. *Int J Clin Exp Med* 2015; 8:13118–13126.
9. Cheng KL, Choi YJ, Shim WH, Lee JH, Baek JH. Virtual touch tissue imaging quantification shear wave elastography: prospective assessment of cervical lymph nodes. *Ultrasound Med Biol* 2016; 42:378–386. [\[CrossRef\]](#)
10. Ben Z, Gao S, Wu W, et al. Clinical value of the VTIQ technology in the differential diagnosis of superficially enlarged lymph nodes. *Acta Radiol* 2018; 59:836–844. [\[CrossRef\]](#)
11. Azizi G, Keller JM, Mayo ML, et al. Shear wave elastography and cervical lymph nodes: predicting malignancy. *Ultrasound Med Biol* 2016; 42:1273–1281. [\[CrossRef\]](#)
12. Zhao Y, Xi J, Zhao B, et al. Preliminary evaluation of virtual touch tissue imaging quantification for differential diagnosis of metastatic and nonmetastatic cervical lymph nodes. *J Ultrasound Med* 2017; 36:557–563. [\[CrossRef\]](#)
13. Som PM, Curtin HD, Mancuso AA. Imaging-based nodal classification for evaluation of neck metastatic adenopathy. *AJR Am J Roentgenol* 2000; 174:837–844. [\[CrossRef\]](#)
14. Tozaki M, Saito M, Benson J, Fan L, Isobe S. Shear wave velocity measurements for differential diagnosis of solid breast masses: a comparison between virtual touch quantification and virtual touch IQ. *Ultrasound Med Biol* 2013; 39:2233–2245. [\[CrossRef\]](#)
15. Hajek PC, Salomonowitz E, Turk R, Tscholakoff D, Kumpan W, Czembirek H. Lymph nodes of the neck: evaluation with US. *Radiology* 1986; 158:739–742. [\[CrossRef\]](#)
16. Shozushima M, Suzuki M, Nakasima T, Yanagisawa Y, Sakamaki K, Takeda Y. Ultrasound diagnosis of lymph node metastasis in head and neck cancer. *Dentomaxillofac Radiol* 1990; 19:165–170. [\[CrossRef\]](#)
17. Ganeshalingam S, Koh DM. Nodal staging. *Cancer Imaging* 2009; 9:104–111. [\[CrossRef\]](#)
18. Vassallo P, Edel G, Roos N, Naguib A, Peters PE. In-vitro high-resolution ultrasonography of benign and malignant lymph nodes. A sonographic-pathologic correlation. *Invest Radiol* 1993; 28:698–705. [\[CrossRef\]](#)
19. Ying M, Ahuja A, Brook F, Brown B, Metreweli C. Nodal shape (S/L) and its combination with size for assessment of cervical lymphadenopathy: which cut-off should be used? *Ultrasound Med Biol* 1999; 25:1169–1175. [\[CrossRef\]](#)
20. Alam F, Naito K, Horiguchi J, Fukuda H, Tachikake T, Ito K. Accuracy of sonographic elastography in the differential diagnosis of enlarged cervical lymph nodes: comparison with conventional B-mode sonography. *AJR Am J Roentgenol* 2008; 191:604–610. [\[CrossRef\]](#)
21. Lyschchik A, Higashi T, Asato R, et al. Cervical lymph node metastases: diagnosis at sonoelastography—initial experience. *Radiology* 2007; 243:258–267. [\[CrossRef\]](#)
22. Papakonstantinou O, Bakantaki A, Paspalaki P, Charoulakis N, Gourtsoyiannis N. High-resolution and color Doppler ultrasonography of cervical lymphadenopathy in children. *Acta Radiol* 2001; 42:470–476. [\[CrossRef\]](#)
23. Ahuja A, Ying M. Sonography of neck lymph nodes. Part II: abnormal lymph nodes. *Clin Radiol* 2003; 58:359–366. [\[CrossRef\]](#)
24. Ying M, Ahuja AT, Evans R, King W, Metreweli C. Cervical lymphadenopathy: sonographic differentiation between tuberculous nodes and nodal metastases from non-head and neck carcinomas. *J Clin Ultrasound* 1998; 26:383–389.
25. Ahuja A, Ying M, Yang WT, Evans R, King W, Metreweli C. The use of sonography in differentiating cervical lymphomatous lymph nodes from cervical metastatic lymph nodes. *Clin Radiol* 1996; 51:186–190. [\[CrossRef\]](#)
26. Ahuja A, Ying M, King W, Metreweli C. A practical approach to ultrasound of cervical lymph nodes. *J Laryngol Otol* 1997; 111:245–256. [\[CrossRef\]](#)
27. Ahuja A, Ying M, Evans R, King W, Metreweli C. The application of ultrasound criteria for malignancy in differentiating tuberculous cervical adenitis from metastatic nasopharyngeal carcinoma. *Clin Radiol* 1995; 50:391–395. [\[CrossRef\]](#)
28. Ying M, Ahuja A, Brook F. Sonographic appearances of cervical lymph nodes: variations by age and sex. *J Clin Ultrasound* 2002; 30:1–11. [\[CrossRef\]](#)
29. Ahuja AT, Chow L, Chick W, King W, Metreweli C. Metastatic cervical nodes in papillary carcinoma of the thyroid: ultrasound and histological correlation. *Clin Radiol* 1995; 50:229–231. [\[CrossRef\]](#)
30. DePena CA, Van Tassel P, Lee YY. Lymphoma of the head and neck. *Radiol Clin North Am* 1990; 28:723–743.
31. Sakaguchi T, Yamashita Y, Katahira K, et al. Differential diagnosis of small round cervical lymph nodes: comparison of power Doppler US with contrast-enhanced CT and pathologic results. *Radiat Med* 2001; 19:119–125.
32. Ahuja AT, Ying M, Ho SS, Metreweli C. Distribution of intranodal vessels in differentiating benign from metastatic neck nodes. *Clin Radiol* 2001; 56:197–201. [\[CrossRef\]](#)

33. Ariji Y, Kimura Y, Hayashi N, et al. Power Doppler sonography of cervical lymph nodes in patients with head and neck cancer. *AJNR Am J Neuroradiol* 1998; 19:303–307.
34. Wu CH, Chang YL, Hsu WC, Ko JY, Sheen TS, Hsieh FJ. Usefulness of Doppler spectral analysis and power Doppler sonography in the differentiation of cervical lymphadenopathies. *AJR Am J Roentgenol* 1998; 171:503–509. [\[CrossRef\]](#)
35. Ying M, Ahuja A, Brook F. Accuracy of sonographic vascular features in differentiating different causes of cervical lymphadenopathy. *Ultrasound Med Biol* 2004; 30:441–447. [\[CrossRef\]](#)
36. Zhang JP, Liu HY, Ning CP, Chong J, Sun YM. Quantitative analysis of enlarged cervical lymph nodes with ultrasound elastography. *Asian Pac J Cancer Prev* 2015; 16:7291–7294. [\[CrossRef\]](#)
37. Zhang P, Zhang L, Zheng S, Yu C, Xie M, Lv Q. Acoustic radiation force impulse imaging for the differentiation of benign and malignant lymph nodes: a systematic review and meta-analysis. *PLoS One* 2016; 11:e0166716. [\[CrossRef\]](#)
38. Suh CH, Choi YJ, Baek JH, Lee JH. The diagnostic performance of shear wave elastography for malignant cervical lymph nodes: A systematic review and meta-analysis. *Eur Radiol* 2017; 27:222–230. [\[CrossRef\]](#)
39. Kansal R, Singleton TP, Ross CW, Finn WG, Padmore RF, Schnitzer B. Follicular hodgkin lymphoma: a histopathologic study. *Am J Clin Pathol* 2002; 117:29–35. [\[CrossRef\]](#)
40. Bhatia K, Tong CS, Cho CC, Yuen EH, Lee J, Ahuja AT. Reliability of shear wave ultrasound elastography for neck lesions identified in routine clinical practice. *Ultraschall Med* 2012; 33:463–468. [\[CrossRef\]](#)